Pressure anisotropy effects on nonlinear electrostatic excitations in magnetized electron-positron-ion plasmas

Muhammad Adnan[1,2], Gina Williams[2], Anisa Qamar[1], S. Mahmood[3] and Ioannis Kourakis[2]
[1] *Institute of Physics and Electronics, University of Peshawar, Peshawar 25000, Pakistan*

[2] *Department of Physics and Astronomy, Centre for Plasma Physics, Queen's University Belfast, BT7 1NN Northern Ireland, United Kingdom*

[3] *Theoretical Physics Division (TPD), PINSTECH P.O. Nilore Islamabad 44000 Pakistan*

(Dated: June 20, 2014)

The propagation of linear and nonlinear electrostatic waves is investigated in a magnetized anisotropic electron-positron-ion (e-p-i) plasma with superthermal electrons and positrons. A two-dimensional plasma geometry is assumed. The ions are assumed to be warm and anisotropic due to an external magnetic field. The anisotropic ion pressure is defined using the double adiabatic Chew-Golberger-Low (CGL) theory. In the linear regime, two normal modes are predicted, whose characteristics are investigated parametrically, focusing on the effect of superthermality of electrons and positrons, ion pressure anisotropy, positron concentration and magnetic field strength. A Zakharov-Kuznetsov (ZK) type equation is derived for the electrostatic potential (disturbance)s via a reductive perturbation method. The parametric role of superthermality, positron content, ion pressure anisotropy and magnetic field strength on the characteristics of solitary wave structures is investigated. Following Allen and Rowlands [M. A. Allen and G. Rowlands, J. Plasma Phys. **53**, 63 (1995)], we have shown that the pulse soliton solution of the ZK equation is unstable to oblique perturbations, and have analytically traced the dependence of the instability growth rate on superthermality and ion pressure anisotropy.

I. INTRODUCTION

In a collisionless medium, the presence of strong magnetic field makes the plasma anisotropic, i.e., it behaves differently in the parallel and perpendicular direction relative to the external magnetic field [1]. The CGL theory [2] also known as double adiabatic theory, presented by Chew-Goldberger-Low (CGL) in 1956 is applicable to such anisotropic plasma provided no coupling exists between the parallel and perpendicular degrees of freedom [3]. To describe anisotropic plasma situations, one needs two separate equations of state to evaluate the ion pressure i.e., $p_{\|i}$ and $p_{\perp i}$, where $p_{\|i}$ ($p_{\perp i}$) are the parallel (perpendicular, respectively) component of the ion pressure relative to the ambient magnetic field. Such anisotropy may be smeared out if there's a strong correlation between the parallel and perpendicular directions due to wave-particle interactions [4, 5]. In Space plasmas, there are situations where plasma convection results in magnetic compression and/or expansion along the field lines. The magnetic compression leads to an increase in the perpendicular temperature $T_\perp$ (relative to magnetic field) of the particles while expansion leads to a decrease in the parallel temperature $T_\|$ [4]. This mechanism results in temperature anisotropy i.e., $T_{\perp i}/T_{\|i} \neq 1$. Relevant examples include stream-stream (fast and slow streams of charged particles) interaction in the solar wind, sunward flow in the terrestrial and planetary magnetotails and magnetosheath flow in terrestrial and planetary magnetospheres [4].

Electrostatic solitary waves have been studied since long ago by assuming a Maxwellian particle distribution for the electron background. However it is well established now by evidence from both Space [6–9] and laboratory [10, 11] plasmas, that non-Maxwellian particle distributions are required to model efficiently the role of energetic particles, associate with long-tailed (superthermal) velocity distributions. Such particles are efficiently modeled by a generalized Lorentzian velocity distribution function or a kappa distribution. The form of the kappa distribution was postulated by Vasyliunas in 1968 [6] to fit observational solar wind data. By now, the kappa distribution has been employed to describe many astrophysical and Space plasma situations, e.g. in the auroral zone [12], in the Earth's magnetosphere [13], in the interstellar medium [14] and the solar wind [15]. Interestingly, non-Maxwellian particles are also observed in the lab [10, 11].

Extensive research has recently been devoted to the effect of superthermal electron distribution on solitary waves [16–19]. Saini *et al.* [20] have investigated the dynamics of electrostatic solitary excitations in the presence of superthermal electrons by using a pseudopotential method, and showed that for a fixed Mach number the profile of solitary waves is steeper and wider than the usual structures occurring in plasmas. A nonlinear Schrödinger equation formalism was later employed to describe the role of superthermal particles on electrostatic wavepackets in electron-ion [21] and electron-

positron-ion [22] plasmas, revealing that superthermality increases the modulational instability of such wavepackets. The linear and nonlinear dynamics of multidimensional excitations in the presence of superthermal electrons were recently investigated by Williams and Kourakis [23]. Ion thermal effects on ion acoustic waves propagating in a magnetized superthermal plasma have recently been investigated by Singh *et al* [24], by using Sagdeev potential approach, who thus achieved good agreement with Viking satellite observations in the auroral region.

In order to investigate physical processes of interest involved in the dynamics of real magnetized plasma, there are various theoretical models based on different assumptions and simplifications. Ion pressure anisotropy naturally develops in a low density magnetized plasma, when the gyro-motion (motion in perpendicular plane) and the B-field aligned motion are not coupled by collisions [25]. The magnetic field provides the preferred orientation, while collisional effects (interparticle collisions, or collisions with neutrals) tend to drive the plasma to an isotropic state by evenly distributing the parallel and perpendicular momenta with respect to the magnetic field. If collisionality effects are weak enough (but finite), the parallel and perpendicular components of the ion pressure tensor may differ, although this difference may be bounded by instabilities, like firehose, mirror and cyclotron instabilities [26]. Space plasmas, our primary interest, are basically collisionless and hence ion pressure anisotropy can play an important role. Using a fluid model, Choi *et al* [4] studied solitary waves in a magnetized dusty plasma with anisotropic ion pressure by using the Sagdeev potential method.

Electron positron ion plasmas (e-p-i) have been the focus of various studies in recent years [27–32], due to their occurrence in astrophysical plasma environments, e.g. in the magnetosphere of neutron stars [33], in active galactic cores [34], and in solar flare plasma [35]. Importantly, e-p-i plasmas have also been produced in the laboratory [36–38] and the existence of positrons in other laboratory plasmas has been confirmed [39–41]. The process of electron-positron pair production can occur during the interaction of a strong laser pulse with plasmas [42–45], as well as by the interaction of relativistic superthermal electrons with high-Z material [46]. The creation of large numbers of MeV positrons in the laboratory has led to more antimatter research, including investigation of the physics underlying various astrophysical phenomena such as black holes and gamma ray bursts, positronium production and Bose-Einstein condensates [47, 48]. Pair-plasma production was also studied for underdense plasmas and plasma channels [49], when the number of relativistic electrons can be high, because the laser pulse can propagate a long distance, whereas the density is limited by the critical density for the laser pulse. Various mechanisms can be found for the production of electron-positron pairs by intense focused laser light pulses; see, for example, Refs. 50 and 51. Thus the study of the properties of e-p-i plasmas in the presence of strong and superstrong laser pulses or non-thermal equilibrium cosmic field radiation is of much interest. Currently unpublished results on pair-plasma production via tabletop laser based procedures [52] will generate even more interest on this topic.

The properties of conventional electron-ion plasma change due to the presence of positrons (as *a priori* obvious from the associated ion-to-electron charge misbalance). Importantly, the interaction of high energy gamma ray photons with the atoms/molecules leads to the generation of high energy electrons and positrons in the interstellar medium [53] and the Earth's upper atmosphere [54–57]. Similarly, the plasma sheet boundary of earth magneto-tail also contain such energetic particles (nonthermal) originating partially from the pulsar into the low density interstellar plasma [58–60].

Our work at hand is motivated by a series of observations in the magnetosheath, namely by AMPET/CCF and AMPET/IRM missions, as described in Denton *et al* [5], and also partly by the work of Seough *et al* [26]. Pressure anisotropy also has an essential role in the turbulent intracluster medium (ICM) as discussed by Nakwacki *et al* [61]. They showed that in a low density collisionless medium, such as ICM the thermal pressure become anisotropic with respect to the magnetic field orientation and lead to the evolution of the turbulent gas. The working hypothesis for ion pressure anisotropy to occur in such plasma environments is that the ion gyrofrequency is much larger than the ion-ion collision frequency. Our aim is to provide a working model for solitary wave related phenomena in various space and astrophysical environments in the presence of strong magnetic fields, in particularly to the magnetosphere and to Earth's magnetosheath [4, 5, 61], where non-thermal electrons with ion pressure anisotropy may exist.

In this article, we extend earlier work [62] (in fact also relaxing the plasma neutrality hypothesis adopted therein), with aim to explore the dynamics of small-but-finite amplitude ion acoustic solitary waves in magnetized plasmas characterized by anisotropy and containing superthermal electron and positron components. The paper at hand is organized in the following manner. In section II, we present the basic set of fluid dynamical equations for ion-scale electrostatic excitations in magnetized anisotropic e-p-i plasma. Section III is dedicated to a comprehensive analysis of the linear dynamical regime, and to a discussion of various subcases. A ZK-type evolution equation is derived in section IV, and an analytical solitary wave solution is presented in Section V. Section VI is devoted to a parametric investigation in terms of various plasma parameters of relevance. In Section VII, we have discussed the stability of obliquely propagating solitary waves (obtained as solutions of the ZK equation). Finally, we summarize our results in the concluding Section VIII.

II. FLUID MODEL

We consider the propagation of electrostatic waves in a magnetized, collisionless three component plasma, consisting of hot ions and kappa distributed inertialess electrons and positrons. The ionic pressure tensor is assumed to be anisotropic, with respect to the direction of the ambient magnetic field, and is modelled via the adiabatic or Chew- Golberger-Low (CGL) description [2]. The ambient magnetic field is uniform and assumed to be along the $\hat{x}$-axis i.e. $\mathbf{B} = B_0\widehat{x}$.

The dynamics of the ion fluid is described by the equations:

$$\partial_t n_i + \nabla \cdot (n_i \mathbf{v}_i) = 0 \tag{1}$$

$$\partial_t \mathbf{v}_i + (\mathbf{v}_i \cdot \nabla)\, \mathbf{v}_i = \frac{Ze}{m_i}\mathbf{E} + \frac{Ze}{m_i c}\,(\mathbf{v}_i \times B_0\widehat{x}) - \frac{1}{m_i n_i}\nabla\cdot\widetilde{\mathbf{P_i}}\,. \tag{2}$$

In the case of a strong magnetic field B_0, the plasma becomes anisotropic and behaves differently in the perpendicular and parallel directions, thus the pressure tensor $\widetilde{\mathbf{P_i}}$ takes the form [4, 62]:

$$\widetilde{\mathbf{P_i}} = p_{\perp i}\widehat{\mathbf{I}} + \left(p_{\parallel i} - p_{\perp i}\right)\widehat{\mathbf{b}}\widehat{\mathbf{b}}\,, \tag{3}$$

where $\widehat{\mathbf{I}}$ is the unit tensor and $\widehat{\mathbf{b}}$ is the unit vector along the external magnetic field. The perpendicular and parallel pressure terms are defined as [4, 62]

$$p_{\perp i} = p_{\perp i0}\left(\frac{n_i}{n_{i0}}\right) \qquad \text{and} \qquad p_{\parallel i} = p_{\parallel i0}\left(\frac{n_i}{n_{i0}}\right)^3, \tag{4}$$

where $p_{\perp i0} = n_{i0}T_{i\perp}$ and $p_{\parallel i0} = n_{i0}T_{i\parallel}$ are the equilibrium values of the ion perpendicular and parallel pressure respectively. In the isotropic case, $p_{\parallel i} = p_{\perp i}$, and therefore $\nabla \cdot \widetilde{\mathbf{P_i}} = \nabla p_i$.

The particle density of the electrons and positron components is expressed as

$$n_e = n_{e0}\left[1 - \frac{e\phi}{T_e(\kappa_e - 3/2)}\right]^{-\kappa_e+1/2}$$

and

$$n_p = n_{p0}\left[1 + \frac{e\phi}{T_p(\kappa_p - 3/2)}\right]^{-\kappa_p+1/2} \tag{5}$$

respectively, where κ_e and κ_p are spectral indices measuring the slope of the energy spectrum of the electrons and positrons at the tail of the distribution function, hence the smaller the value of κ_e the stronger the electron concentration in the superthermal region of the distribution function (similarly for positrons). The Maxwellian limit is recovered for infinite κ. The system is closed by Poisson's equation:

$$\nabla \cdot \mathbf{E} = 4\pi e\left(n_i - n_e + n_p\right). \tag{6}$$

The electric field intensity is defined as $\mathbf{E} = -\nabla\phi$, where ϕ is the electrostatic potential (a function of space and time, here). Charge balance at equilibrium requires $n_{i0} + n_{p0} = n_{e0}$.

A. Evolution equations in scalar form

Plasma dynamics is essentially two-dimensional (2D), in this case, since only two direction are of relevance, say $\{\parallel, \perp\} = \{x, y\}$, viz. $\nabla = (\partial_x, \partial_y, 0)$. . In other words, excitations are assumed to evolve and propagate in the xy-plane, with no loss of generality. Then the above system takes the form

$$\partial_t n_i + \partial_x\left(n_i v_{ix}\right) + \partial_y\left(n_i v_{iy}\right) = 0, \tag{7}$$

$$\partial_t v_{ix} + \left(v_{ix}\partial_x + v_{iy}\partial_y\right) v_{ix} = -\frac{e}{m_i}\partial_x\phi - \frac{3p_{\parallel i0}}{m_i n_0^3 n_i} n_i^2 \partial_x n_i, \tag{8}$$

$$\partial_t v_{iy} + \left(v_{ix}\partial_x + v_{iy}\partial_y\right) v_{iy} = -\frac{e}{m_i}\partial_y\phi + \Omega_i v_{iz} - \frac{p_{\perp i0}}{m_i n_0 n_i}\partial_y n_i, \tag{9}$$

$$\partial_t v_{iz} + \left(v_{ix}\partial_x + v_{iy}\partial_y\right) v_{iz} = -\Omega_i v_{iy}, \tag{10}$$

and

$$\partial_x^2\phi + \partial_y^2\phi = 4\pi e\left(n_e - n_p - n_i\right). \tag{11}$$

Here, v_{ix}, v_{iy}, v_{iz} denote the fluid velocity components, the ion gyro-frequency is defined by $\Omega_i = \frac{eB_0}{m_i c}$. The quantities e, m_i, n_e, n_p, n_i, and ϕ represent the electronic charge, ion mass, electron fluid density, positron fluid density and electrostatic potential respectively. Note that the ionic charge state has been set equal to unity, i.e. $Z_i = 1$, everywhere.

B. Dimensionless evolution equations

The above system of equations can be written in normalized form as:

$$\partial_t n_i + \partial_x\left(n_i v_{ix}\right) + \partial_y\left(n_i v_{iy}\right) = 0, \tag{12}$$

$$\partial_t v_{ix} + \left(v_{ix}\partial_x + v_{iy}\partial_y\right) v_{ix} = -\partial_x\Phi - P_\parallel n_i \partial_x n_i, \tag{13}$$

$$\partial_t v_{iy} + \left(v_{ix}\partial_x + v_{iy}\partial_y\right) v_{iy} = -\partial_y\Phi + \Omega v_{iz} - \frac{P_\perp}{n_i}\partial_y n_i, \tag{14}$$

$$\partial_t v_{iz} + \left(v_{ix}\partial_x + v_{iy}\partial_y\right) v_{iz} = -\Omega v_{iy}. \tag{15}$$

In the above relations, the dimensionless parameter Ω denotes the ratio $\Omega = \frac{\Omega_i}{\omega_{pi}}$, while $P_\parallel = \frac{3p_{\parallel i0}}{n_{i0}T_e}$ and $P_\perp =$

$\frac{p_{\perp i0}}{n_{i0}T_e}$ express the relative strength of the pressure (scaled by the thermal pressure) in the respective directions.

Assuming small deviations from the equilibrium state, the particle densities may be expanded as

$$n_e \simeq \delta \left\{1 + c_1\Phi + c_2\Phi^2 + \mathcal{O}(\Phi^3)\right\}, \tag{16}$$

and

$$n_p \simeq p \left\{1 - d_1\Phi + d_2\Phi^2 + \mathcal{O}(\Phi^3)\right\}, \tag{17}$$

where the coefficients c_1, c_2, d_1 and d_2 are functions of the κ parameter(s):

$$c_1 = \left(\frac{\kappa_e - 1/2}{\kappa_e - 3/2}\right), \qquad c_2 = c_1 \frac{\kappa_e + 1/2}{2(\kappa_e - 3/2)},$$
$$d_1 = \sigma_e \left(\frac{\kappa_p - 1/2}{\kappa_p - 3/2}\right), \qquad d_2 = d_1 \frac{\sigma_e(\kappa_p + 1/2)}{2(\kappa_p - 3/2)}. \tag{18}$$

Accordingly, Poisson's equation takes the form:

$$\partial_x^2\Phi + \partial_y^2\Phi \simeq 1 - n_i + \mu\Phi + \nu\Phi^2 . \tag{19}$$

The terms μ and ν are defined as,

$$\mu = (\delta c_1 + p d_1) \text{ and } \nu = (\delta c_2 - p d_2).$$

In the vanishing positron limit ($p = 0$), $\mu \to c_1$ and $\nu \to c_2$; if, furthermore, one takes $\kappa_{e,p} \to \infty$, one is led to $\mu = 2\nu = 1$, as expected [63]. Similarly in the "Maxwellian" e-p-i plasma limit ($\kappa_{e,p} \to \infty$), the expressions for the coefficients reduce to $\mu \to \delta + \sigma_e p$ and $\nu \to 1/2(\delta - \sigma_e^2 p)$.

Overall charge neutrality at equilibrium imposes

$$\delta = 1 + p. \tag{20}$$

we have defined the ratios

$$\delta = n_{e0}/n_{i0} \qquad p = n_{p0}/n_{i0}, \qquad \sigma_e = T_e/T_p ,$$

where n_{e0}, n_{p0} and n_{i0} represent the unperturbed value(s) of the electron, positron and ion densities, while T_e and T_p denote the electron and positron temperature, respectively. Note that c_1, c_2, d_1 and d_2 are positive for all values of κ_e/κ_p greater than 3/2. In writing down the above system, we have adopted the following normalization scheme: the space and time variables are scaled by the ion Debye radius $\lambda_{Di} = \left(k_B T_e/4\pi n_{i0} e^2\right)^{1/2}$ and the inverse ion plasma frequency $\omega_{pi}^{-1} = \left(m_i/4\pi n_{i0} e^2\right)^{1/2}$, respectively; the number density variables n_j (for species $j = e, p, i$) have been scaled by the equilibrium ion density n_{i0}; the electrostatic potential ϕ has been scaled by (T_e/e); the ion fluid speed (components) have been normalized by the ion sound speed $c_s = (T_e/m_i)^{1/2}$.

III. LINEAR ANALYSIS

The standard linear procedure consists of Fourier analyzing Eqs.(12-19), by assuming small perturbations $\sim e^{i(k_x x + k_y y - \omega t)}$. One thus obtains a linear dispersion relation (DR) in the form:

$$1 = \left(\frac{1}{k^2 + \mu} + P_\parallel\right)\frac{k_x^2}{\omega^2} + \left(\frac{1}{k^2 + \mu} + P_\perp\right)\frac{k_y^2}{\omega^2 - \Omega^2}, \tag{21}$$

where $k^2 = k_x^2 + k_y^2$. Recall that $k_x = k_\parallel$ and $k_y = k_\perp$ essentially correspond to the wavenumber (component) in the parallel and perpendicular direction(s), respectively. The structure of the above DR is self-explanatory: one notices the superthermality effect via μ (recovering a Maxwellian limit for $\kappa_{e,p} \to \infty$), as well as the effect of the ion pressure anisotropy through the appearance of (in fact, the difference between) $P_\parallel$ and $P_\perp$. The magnetic field affects the dynamics via its strength, through the ratio Ω (defined above), but also qualitatively, setting up a cylindrical plasma symmetry via the distinct variables k_x and k_y. Equation (21) can be solved for the frequency (square) to give:

$$\omega_\pm^2 = \frac{1}{2}\left[\left(\frac{k^2}{k^2 + \mu} + k_x^2 P_\parallel + k_y^2 P_\perp + \Omega^2\right) \pm \sqrt{\left\{\left(\frac{k^2}{k^2 + \mu} + k_x^2 P_\parallel + k_y^2 P_\perp + \Omega^2\right)^2 - 4\left(\frac{k_x^2}{k^2 + \mu} + P_\parallel k_x^2\right)\Omega^2\right\}}\right], \tag{22}$$

where ω_+ and ω_- ($< \omega_+$) define a fast and a slow electrostatic branch, respectively.

For the sake of rigor, and for later reference, let us point out that the lower branch ("slow" wave), ω_-, defines an acoustic mode, viz. $\omega_- \underset{k\to 0}{\longrightarrow} 0$. In particular, the limit

$$\lim_{k_x \to 0}\left(\frac{\omega_-}{k_x}\right) = \left(\frac{1}{\mu} + P_\parallel\right)^{1/2} \tag{23}$$

provides the phase speed of the magnetoacoustic mode, that is, in fact, the true sound speed for quasi-parallel propagation in the presence of anisotropy, as discussed

in the next section (equation(34)). Note that the latter relation reduces to unity in the limit $P_\parallel = 0$ (cold ions) and $\delta = \mu = 1$ (Maxwellian electrons), i.e. precisely the ion sound speed (in reduced units). The anisotropy of the dynamical problem is manifested by the inequality $P_\parallel \neq P_\perp$, as obvious upon inspection of Eqs. (21)-(22). The upper mode, on the other hand, presents a frequency gap $\omega_+ \to \Omega$ at $k \to 0$ ($k_y = k_x = 0$), and corresponds, physically, to upper-hybrid oscillations. It is interesting to note that, for $k_y \neq k_x = 0$ (i.e. for propagation which is not strictly p), the frequency gap depends on k_y.

A. Asymptotic behavior

It may be appropriate to study the analytical behavior of $\omega_\pm^2$ for large wavelength (small wavenumber) values, based on Eq. (22). Using a Taylor expansion, assuming that both $k_x \equiv k_\parallel \ll 1$ and $k_y \equiv k_\perp \ll 1$ (in scaled units) holds, one may express $\omega_\pm^2$ as

$$\omega_-^2 \approx \left(\frac{1}{\mu} + P_\parallel\right) k_x^2 - \frac{1}{\mu^2}\left[\frac{1+\mu(P_\parallel + P_\perp + \mu P_\parallel P_\perp)}{\Omega^2} + 1\right] k_x^2 k_y^2 + \mathcal{O}(k_x^3, k_y^3)\,, \tag{24}$$

and

$$\omega_+^2 \approx \Omega^2 + \left(\frac{1}{\mu} + P_\perp\right) k_y^2 + \frac{1}{\mu^2}\left[\frac{1+\mu(P_\parallel + P_\perp + \mu P_\parallel P_\perp)}{\Omega^2} - 1\right] k_x^2 k_y^2 + \mathcal{O}(k_x^3, k_y^3). \tag{25}$$

We notice that the former (acoustic) mode is essentially related to parallel propagation, and depends parametrically (weakly) on k_y and on B, viz. the phase speed (square) for parallel propagation is

$$\frac{\omega_-^2}{k_x^2} \approx \frac{1}{\mu} + P_\parallel - \frac{1}{\mu^2}\left[\frac{1+\mu(P_\parallel + P_\perp + \mu P_\parallel P_\perp)}{\Omega^2} + 1\right] k_y^2 + \mathcal{O}(k_x^1, k_y^3)\,; \tag{26}$$

cf. (23). On the other hand, the latter (Langmuir-like, with cutoff) branch is dominant for larger angles, i.e. for strong deviation from the direction of the magnetic field. For perpendicular propagation, viz. $k_x \to 0$, the second mode becomes parabolic, i.e. becomes reminiscent of an electromagnetic magnetic-field dependent mode.

For large $k_x \gg 1$, the lower (acoustic) mode in Eq. (24) saturates as $\omega_-^2 \to \Omega^2$ (zero phase speed for short wavelength), while the upper one (25) goes to infinity as $\omega_+^2 \approx P_\parallel k_x^2$, i.e. results in a thermal mode, sustained by the (parallel component of the) ion pressure.

The above observations will help the reader understand the behavior of the dispersion branches, as depicted in the following.

B. Parametric investigation of the linear dispersion characteristics

It appears imposed to investigate the behavior of our dispersion relation Eq. (22) for different values of the spectral parameter (κ), positron concentration (via p) and magnetic field strength (Ω). These three aspects are shown in the behavior of the two dispersion branches versus the parallel wavenumber (component) k_x, as depicted in Figure 1. It can be seen from Fig. 1a that the frequencies of both branches decrease with lower value of κ, i.e. for stronger deviations from the Maxwellian reference state (and, in fact, this effect is more visible on the fast mode). Figure 1b depicts the effect of positron concentration p on the frequencies based on the dispersion relation described by Eq. (22). It is evident that increasing the positron concentration tends to decrease the frequencies of both the fast and slow modes as shown in figure 1(b). In Figure 1c, we have shown how the dispersion curve changes with varying magnetic field strength (through Ω). The acoustic mode (lower branch) increases its phase speed as Ω goes higher, for small values of k_x, and eventually attains a constant asymptotic value at large k_x. On the other hand, the cyclotron mode (upper branch) increases sharply at small value of k_x with Ω, and then the curve converges to a linear behavior for larger k_x. The above observations could also be predicted from the information in the previous subsection: e.g., cf. (24) and (25).

In Figure 2 we have investigated the effects of ion pressure anisotropy (via $P_\parallel$, $P_\perp$) on the dispersion relation. Figure 2a exhibits how the parallel (ionic) pressure $P_\parallel$ affect the frequencies in the fast and slow modes in the case when $P_\parallel$ is greater than its perpendicular counterpart $P_\perp$, i.e., $P_\parallel > P_\perp$. It is clear that for a fixed value of $P_\perp$, an increase in $P_\parallel$ leads to an increase in the frequency of both modes. On the other hand, considering the case $P_\perp > P_\parallel$ now, by keeping $P_\parallel$ fixed and increasing the perpendicular pressure $P_\perp$, one observes the opposite trend in $P_\perp$, as shown in figure 2b: increasing $P_\perp$ results in enhancement of the upper mode (frequency), while it slows down the lower mode; in other words, the effect of $P_\perp$

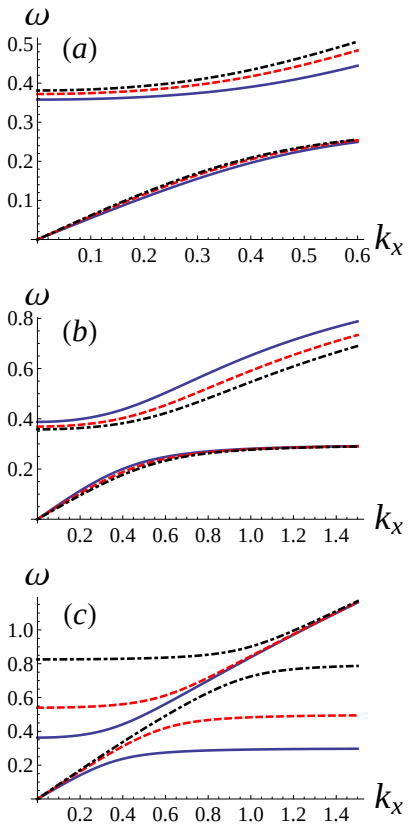

FIG. 1: Dispersion relation based on Eq. (22) for $k_y = 0.3$, $\sigma_e = 1$, with:
(a) (Upper panel) $P_\parallel = 0.02, P_\perp = 0.01, p = 0.2, \Omega = 0.3$, and: $\kappa_e = \kappa_p = \kappa = 3$ (blue solid lines), $\kappa_e = \kappa_p = \kappa = 5$ (red dashed lines), $\kappa_e = \kappa_p = \kappa = 10$ (black dot-dashed lines);
(b) (Middle panel) $P_\parallel = 0.01$, $P_\perp = 0.1, \Omega = 0.3, \kappa_e = \kappa_p = \kappa = 3$, and: $p = 0$ (blue solid lines), $p = 0.2$ (red dashed lines), $p = 0.4$ (black dot-dashed lines);
(c) (Lower panel) $p = 0.2, \kappa_e = \kappa_p = \kappa = 3$, $P_\parallel = 0.375$, $P_\perp = 0.05$, and: $\Omega = 0.3$ (blue solid lines), $\Omega = 0.5$ (red dashed lines), $\Omega = 0.8$ (black dot-dashed lines).

($> P_\parallel$) consists in separating the two modes. These observations agree, qualitatively speaking, with Eqs. (24) and (25) above.

Let us highlight some of the important features of Figure 2a and 2b. In Fig. 2a, one can see that the frequencies in the fast mode do not change with $P_\parallel$ for very small k_x and yet increase sharply for larger k_x. In the lower mode, the frequencies vary with $P_\parallel$ for $k_x \to 0$ but attain a constant saturated values at larger k_x. Similarly in Figure 2b, we can see that the effect of $P_\perp$ on the lower mode is dominant in the short wavelength limit (large k_x), while it bears a constant effect on the upper mode for all k_x. The numerical values of $P_\parallel$ and $P_\perp$ are chosen such that we do not exceed the limits of $T_{i\perp}$ and $T_{i\parallel}$ plotted in Ref. 26; furthermore, when considering the ion pressure anisotropy cases (i.e., the relative strength of $P_\parallel \neq P_\perp$), we have employed data from Ref. 5.

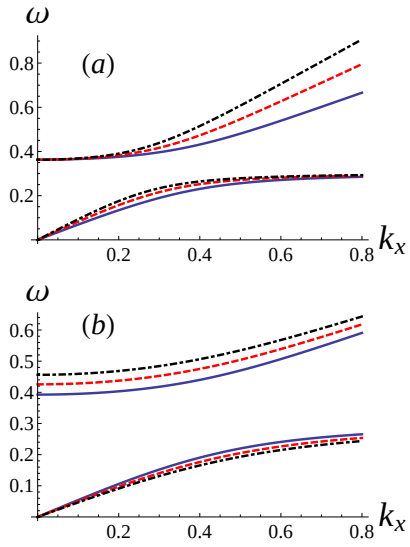

FIG. 2: Dispersion relation based on Eq. (22) for $k_y = 0.3$, $\sigma_e = 1$, $p = 0.2$, $\Omega = 0.3$ and $\kappa_e = \kappa_p = \kappa = 3$, with:
(a) (Upper panel) $P_\perp = 0.05$, $P_\parallel = 0.3$ (blue solid lines), $P_\parallel = 0.6$ (red dashed lines), $P_\parallel = 0.9$ (black dot-dashed lines);
(b) (Middle panel) $P_\parallel = 0.1$, $P_\perp = 0.3$ (blue solid lines), $P_\perp = 0.6$ (red dashed lines), $P_\perp = 0.9$ (black dot-dashed lines).

C. Limiting Cases

It may be appropriate here, to consider some special cases. We point out that all known related physical systems are rigorously recovered as special cases from our algebraic analysis above, in the appropriate limit.

a. Electron-ion plasma. Our results apply in the e-i limit (i.e., for $p = 0$ and $\delta = 1$), where Eq. (13) in Ref. 62 is precisely recovered in the small k limit (in account of the neutrality hypothesis adopted therein). Our results thus extend those of Ref. 62 for larger k, beyond the plasma approximation.

b. Cold-ion model. The cold-ion-electron case considered in Ref. 23 is recovered here, for $p = P_\parallel = P_\perp = 0$ and setting $\Omega = 0$ (for unmagnetized plasma), thus recovering the dispersion relation $\omega^2 = \frac{k_x^2}{k^2+\mu}$.

c. Maxwellian-electron isotropic plasma. The case of Maxwellian-electron-ion plasma with isotropic ion pressure treated in Ref. 64 is recovered here, upon formally considering $p = 0$, $c_1 \to 1$ (i.e., $\kappa_e \to \infty$) and $\nabla \cdot \widetilde{\mathbf{P_i}} = \nabla p_i$, viz., $p_{i\perp} = p_{i\parallel}$. In this case, we obtain:

$$\omega^4 - \left(\frac{k^2}{k^2+1} + \sigma k^2 + \Omega^2\right)\omega^2 + \left(\frac{k_x^2}{k^2+1} + \sigma k_x^2\right)\Omega^2 = 0, \tag{27}$$

where σ here represents the temperature ratio T_i/T_e. In the limit $k \ll 1$, one obtains the result of Ref. 64, yet here extended to larger values of k (since Poisson's equation was adopted in our work, instead of the simplistic plasma approximation [64]).

d. Parallel propagation. Wave propagation parallel to the magnetic field may be considered by taking $k_y \longrightarrow 0$ (thus $k_x = k$), whence Eq. (22) becomes,

$$\omega^2(k) = \frac{k^2}{k^2+\mu} + P_\parallel k^2 \,. \tag{28}$$

This is the dispersion relation for parallel propagating electrostatic waves in a hot magnetized plasma, with superthermal electrons and positrons. It is evident that neither the magnetic field strength, nor ion pressure anisotropy, though both formally considered here, affect the characteristics for parallel propagation, i.e., Ω and P_2 do not appear in the latter relation. The true sound speed in the parallel direction to the magnetic field is thus given by considering the phase speed in (28) for small k, which readily recovers Eq. (23) [or Eq. (34)] above, as expected.

e. Perpendicular propagation. Considering $k_x \longrightarrow 0$ (thus, $k_y = k$) in Eq. (22), leads to

$$\omega^2(k) = \Omega^2 + \frac{k^2}{k^2+\mu} + P_\perp k^2, \tag{29}$$

for magnetoacoustic waves in anisotropic superthermal e-p-i plasma. One clearly distinguishes the effect of the magnetic field, in the second, of the plasma configuration (via μ), in the second, and of $P_\perp$ in the thermally driven last term (sole to survive for infinitely large k).

IV. NONLINEAR ANALYSIS

In this section, we shall investigate the nonlinear behavior of electrostatic waves in anisotropic magnetized e-p-i plasma with suprathermal electron and positron distribution. We adopt the reductive perturbation method [65], by considering a "stretching" (rescaling) of the independent variables as:

$$X = \varepsilon^{1/2}\left(x - \lambda t\right), \qquad Y = \varepsilon^{1/2} y, \qquad \tau = \varepsilon^{3/2} t, \tag{30}$$

where ε is a small expansion parameter($0 < \varepsilon \ll 1$), and λ represents the wave phase velocity, to be determined later. Accordingly, the state variables are expanded as

$$\begin{aligned} n_i &\simeq 1 + \varepsilon n_{i1} + \varepsilon^2 n_{i2} + \varepsilon^3 n_{i3} + \cdots \\ v_{ix} &\simeq \varepsilon v_{ix1} + \varepsilon^2 v_{ix2} + \varepsilon^3 v_{ix3} + \cdots \\ v_{iy} &\simeq \varepsilon^{3/2} v_{iy1} + \varepsilon^2 v_{iy2} + \varepsilon^{5/2} v_{iy3} + \cdots \\ v_{iz} &\simeq \varepsilon^{3/2} v_{iz1} + \varepsilon^2 v_{iz2} + \varepsilon^{5/2} v_{iz3} + \cdots \\ \Phi &\simeq \varepsilon \Phi_1 + \varepsilon^2 \Phi_2 + \varepsilon^3 \Phi_3 + \cdots \end{aligned} \tag{31}$$

where the meaning of the various quantities is obvious. Note that the transverse components (v_{iy}, v_{iz}) of the ion fluid speed appear to evolve more slowly (at higher order in ε) than the parallel velocity component v_{ix}; gyromotion is thus treated as higher order effect.

Substituting the above scaling ansatz into the evolution Eqs. (12)- (19) and collecting terms arising in lowest order $\left(\sim \varepsilon^{3/2}\right)$, we obtain

$$\begin{aligned} v_{ix1} &= \lambda n_{i1}, \\ \partial_X \mathbf{v}_{ix1} &= \frac{1}{\lambda}\left(\partial_X \Phi_1 + P_\parallel \partial_X n_{i1}\right), \\ v_{iy1} &= 0, \\ v_{iz1} &= \frac{1}{\Omega}\left(\partial_Y \Phi_1 + P_\perp \partial_Y n_{i1}\right). \end{aligned} \tag{32}$$

To lowest order ($\sim \varepsilon$), Poisson's equation leads to

$$n_{i1} = \mu \Phi_1. \tag{33}$$

Combining the latter expressions, one may determine the (lowest-orded) pulse propagation speed λ,

$$\lambda = \left(\frac{1}{\mu} + P_\parallel\right)^{1/2}, \tag{34}$$

which thus comes out to be precisely the sound speed, as extracted from our linear analysis earlier; cf. Eq. (23). Note that the value of the (true) sound speed depends on superthermality (through c_1, d_1 involving κ) and on the positron concentration through p, along with the ion pressure $P_\parallel$. (Importantly, the phase velocity of the ion acoustic wave λ is independent of the perpendicular pressure component ($P_\perp$).) In the limit $\kappa_{e,p} \to \infty$, and assuming cold ions, the above expression gives $\lambda \to 1$, which represents the normalized sound speed in Maxwellian conditions.

In Figure (3) we have shown how the phase velocity λ varies with superthermality under the effect of positron concentration and parallel ion pressure $P_\parallel$. One can see that, for lower values of κ (strong superthermality) the phase velocity is reduced, while as $\kappa \to \infty$, the phase velocity asymptotically approaches a constant value, viz. $\lambda \to \sqrt{P_\parallel}$, suggesting a pressure-driven "thermal" wave. We observe that increasing the value of p (positron content) suppresses the phase velocity curves, while on the other hand, increasing $P_\parallel$ leads to an increase in λ. These results are in agreement with the discussion accompanying our lines analysis above; cf. Figs. 1-2.

Collecting the next higher-order $\left(\sim \varepsilon^{5/2}\right)$ contribution from the ion continuity equation, we obtain

$$-\lambda \partial_X n_{i2} + \partial_Y v_{iy2} + \partial_X v_{ix2} = -\partial_\tau n_{i1} - \partial_X\left(n_{i1} v_{ix1}\right). \tag{35}$$

Similarly, the next higher-order contributions from the (three components of the) ion momentum equation are, respectively:

$$\begin{aligned} -\lambda \partial_X v_{ix2} + \partial_X \Phi_2 + P_\parallel \partial_X n_{i2} = &-\partial_\tau v_{ix1} - v_{ix1}\partial_X v_{ix1} \\ &- P_\parallel n_{ix1} \partial_X n_{ix1}, \end{aligned} \tag{36}$$

$$v_{iy2} = \frac{\lambda}{\Omega}\partial_X v_{iz1} \qquad \text{and} \qquad v_{iz2} = -\frac{\lambda}{\Omega}\partial_X v_{iY1}. \tag{37}$$

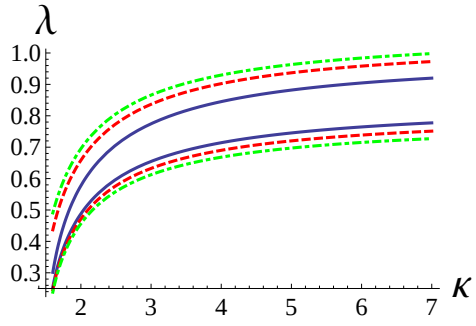

FIG. 3: Plot of the phase velocity λ against κ for $\sigma_e = 1$ and:
(a) (top curves) $p = 0, P_{\|} = 0$ (blue solid line), $P_{\|} = 0.1$ (red dashed line), $P_{\|} = 0.15$ (green dot-dashed line);
(b) (bottom curves) $P_{\|} = 0, p = 0.2$ (blue solid line), $p = 0.3$ (red dashed line), $p = 0.4$ (green dot-dashed line).

In order $\left(\sim \varepsilon^2\right)$, Poisson's equation yields

$$\mu\Phi_2 - n_{i2} = \partial_X^2\Phi_1 + \partial_Y^2\Phi_1 - \nu\Phi_1^2. \tag{38}$$

Eliminating the second-order perturbed quantities and making use of the first order results, we obtain a nonlinear partial derivative equation (PDE) in the form of the Zakharov-Kuznetsov (ZK) equation,

$$\frac{\partial\Phi_1}{\partial\tau} + A\Phi_1\frac{\partial\Phi_1}{\partial X} + \frac{\partial}{\partial X}\left(B\frac{\partial^2\Phi_1}{\partial^2 X} + C\frac{\partial^2\Phi_1}{\partial^2 Y}\right) = 0\,. \tag{39}$$

The real coefficients A (accounting for nonlinearity), B and C (dispersion) are given by:

$$\begin{aligned} A &= B\left[\mu^2\left(3 + 4\mu P_{\|}\right) - 2\nu\right], \\ B &= \frac{1}{2}\frac{1}{\mu^{3/2}\sqrt{1+\mu P_{\|}}}, \\ C &= B\left[1 + \frac{\left(1+\mu P_{\|}\right)\left(1+\mu P_{\perp}\right)}{\Omega^2}\right]. \end{aligned} \tag{40}$$

We point out that A and B do not depend on the perpendicular ion pressure component ($P_{\perp}$), as expected, since quasi-parallel solitary wave propagation was essentially considered (recall the scaling ansatz (30) adopted above).

We add, for rigor, that in all of the limiting cases discussed earlier, our results match with previous works. For example, in the absence of positrons ($p = 0$), Eq. (40) agrees with Eq. (31) in Ref. 62. In the cold-ion limit, we exactly recover the expressions in Ref. 23. In the Maxwellian limit (for both electrons and positrons), viz. $\kappa_{e,p} \longrightarrow \infty$ (i.e., $c_1 = 2c_2 = d_1 = 2d_2 = 1$), we find

$$\begin{aligned} A &= B[(1+2p)^2\{4(1+2p)P_{\|} + 3)\} - 1], \\ B &= \frac{1}{2}\left[\frac{(1+2p)^{-3/2}}{\sqrt{1+P_{\|}(1+2p)}}\right], \\ C &= B\left[1 + \frac{\{1+P_{\|}(1+2p)\}\{1+P_{\perp}(1+2p)\}}{\Omega^2}\right], \end{aligned} \tag{41}$$

The electron-ion case is obtained from the latter expressions upon setting $p = 0$ (no positrons), as

$$\begin{aligned} A &= B(4P_{\|} + 2), \\ B &= \frac{1}{2}\left[\frac{1}{\sqrt{1+P_{\|}}}\right], \\ C &= B\left[1 + \frac{(1+P_{\|})(1+P_{\perp})}{\Omega^2}\right]. \end{aligned} \tag{42}$$

At this stage, one may readily recover the textbook limit expression for A, B and C [66], for $P_{\|} = P_{\perp} = 0$, i.e.

$$A = 1, \qquad B = \frac{1}{2}, \qquad C = \frac{1}{2}\left(1 + \frac{1}{\Omega^2}\right). \tag{43}$$

V. SOLITARY WAVE SOLUTION

A standard qualitative approach to modeling a localized electrostatic excitation consists in considering a pulse-shaped solitary wave solution of the ZK equation (39), in analogy with the (one-dimensional) Korteweg-de Vries (KdV) picture [66]. This may be obtained by using the hyperbolic tangent (tanh) method [67]. According to this method, one considers the variable transformation $\xi = \chi\left(l_x X + l_y Y - u_0\tau\right)$, where χ denotes the inverse of the soliton width and u_0 represents the pulse velocity increment above the sound speed. Here, l_x and l_y are the directional cosines of the wave vector $\mathbf{k}$ along the X and Y directions, respectively, satisfying $l_x^2 + l_y^2 = 1$.

Considering vanishing asymptotic values at infinity, one obtains the analytical solution:

$$\Phi_1 = \Phi_m \mathrm{sech}^2(\xi). \tag{44}$$

Details on the algebraic procedure can be found in Appendix A of Ref. 23, thus including these here is deemed unnecessary. Note that the KdV soliton solution [66] is readily obtained upon setting $l_y = 0$ in Eq.(44).

It is clear from the above solution that the maximum value of the amplitude $\Phi_m = \frac{3u_0}{l_x A}$ is determined by the nonlinearity coefficient A, while the width of the solitary wave structure $W = \chi^{-1} = \sqrt{\frac{4l_x\left(Bl_x^2 + Cl_y^2\right)}{u_0}}$ depends on the dispersive coefficients B and C.

It is important to mention here, that the perturbation method adopted here assumes a finite obliqueness in the wave propagation direction with respect to the magnetic field (expressed via an angle $\theta = \tan^{-1}(l_y/l_x)$); nonetheless, the model breaks down for purely transverse propagation ($l_x = 0$) [68].

The electric field disturbance $\mathbf{E} = -\nabla\Phi_1$ reads

$$\mathbf{E} = \begin{pmatrix} E_X \\ E_Y \end{pmatrix} = 2\Phi_m\chi\mathrm{sech}^2(\xi)\tanh(\xi)\begin{pmatrix} l_{\hat{x}} \\ l_{\hat{y}} \end{pmatrix}. \tag{45}$$

Interestingly, only positive potential pulses are predicted though the above analysis: to see this,

note that the polarity of the pulse in Eq.(44) is prescribed by the sign of the nonlinearity coefficient A in Eq.(41), which is here positive. It must be pointed out, for rigor, that the predictions resulting from the perturbative small-amplitude approach adopted here is not conclusive in what regards the pulse polarity. In fact, in general, space plasma observation reveal solitons (pulses) of either positive or negative polarity. This actually depends on the physics of the plasma, that is, actually on the plasma configuration (constituents, concentration, inertial versus e.g. stationary species, and so on). This polarity coexistence is neatly predicted by (large-amplitude) the Sagdeev pseudopotential theory [69–72]. On the other hand, small-amplitude methods (reductive perturbation techniques) account for weakly superacoustic pulses only, and actually predict only one or the other (plus/minus) polarity, thus failing to describe the polarity reversal in a given plasma configuration. However straightforward to show in 1D, the Sagdeev-type analysis in a 2D/3D geometry is rather tedious and involves physical constraints (e.g. adopting the neutrality hypothesis, for the sake of analytical tractability; refer to the discussion in [73]. We have chosen to proceed with the above analysis in the following, leaving a detailed large-amplitude analysis for a future work.

VI. PARAMETRIC INVESTIGATION

We recall that the nonlinearity coefficient A depends on superthermality (through κ), on the positron concentration (via p) and on the parallel ion pressure $P_\parallel$. On the other hand, the dispersive coefficients B and C are functions of kappa, of the parallel ion pressure components ($P_\parallel$, $P_\perp$), and also depend on the positron content through p. Furthermore, C (only) depends on the magnetic field strength through Ω. We have seen above that the value of these coefficients affects the structural characteristics of the pulse. It is thus appropriate to investigate how the value of these coefficients varies with respect to these parameters.

A. Effect of superthermal particles

In this section we have plotted coefficient A, B and C against the superthermality parameter (assuming $\kappa_e = \kappa_p = \kappa$ for simplicity), focusing successively on the effect(s) of positron concentration, parallel ion pressure and magnetic field.

In Figure 4, we have depicted the effect of superthermality on the coefficients A, B and C, for different values of positron concentration. It is observed that stronger superthermality (lower value of κ) leads to higher A, but to lower B and C values. For large κ, all coefficients tend to constant values, as predicted in the previous Section (discussion about the Maxwellian limit).

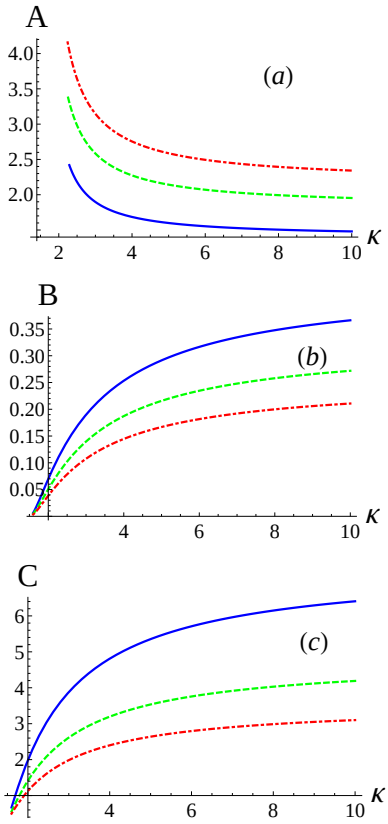

FIG. 4: The coefficients A, B and C are depicted against κ ($= \kappa_e = \kappa_p$, assumed for simplicity), focusing on the positron concentration effect. Here, $P_\parallel = 0.3$, $\sigma_e = 1$, $\Omega = 0.3$. (a) Nonlinearity coefficient A versus κ, for $p = 0$ (blue solid line), $p = 0.2$ (green dashed line), and $p = 0.4$ (red dot-dashed line); (b) Parallel dispersion coefficient B versus κ, for $p = 0$ (blue solid line), $p = 0.2$ (green dashed line), and $p = 0.4$ (red dot-dashed line); (c) Parallel dispersion coefficient C against κ, for $p = 0$ (blue solid line), $p = 0.2$ (green dashed line), and $p = 0.4$ (red dot-dashed line).

A variation in positron content bears the reverse effect on the (value of the) coefficients. It is clear from Figure 4, that by increasing the value of p, the nonlinear coefficient A tends to increase, while the dispersive coefficients B and C is suppressed.

In Figure 5 we have plotted the coefficients A and B against κ, but this time focusing on the effect of the parallel pressure $P_\parallel$. We observe that, for all values of kappa (κ), increasing $P_\parallel$ leads to an increase in the nonlinearity coefficient A, but to a decrease in the dispersive coefficient B (and, consequently, C).

From Eq. (40) it is clear that coefficients A and B are independent of the ion perpendicular pressure $P_\perp$. The perpendicular dispersion coefficient C, on the other hand, has a strong dependence on $P_\perp$ and on the mag-

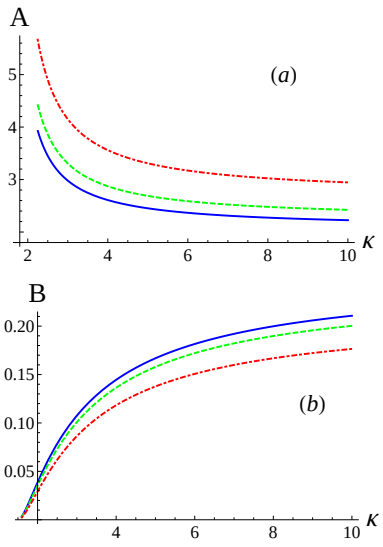

FIG. 5: Plot of A and B versus κ, focusing on the effect of $P_{\|}$. We have assumed $\sigma_e = 1$. (a) A versus κ, for $P_{\|} = 0.3$ (blue solid line), $P_{\|} = 0.4$ (green dashed line), $P_{\|} = 0.7$ (red dot-dashed line). (b) B versus κ, for $P_{\|} = 0.3$ (blue solid line), $P_{\|} = 0.4$ (green dashed line), $P_{\|} = 0.7$ (red dot-dashed line).

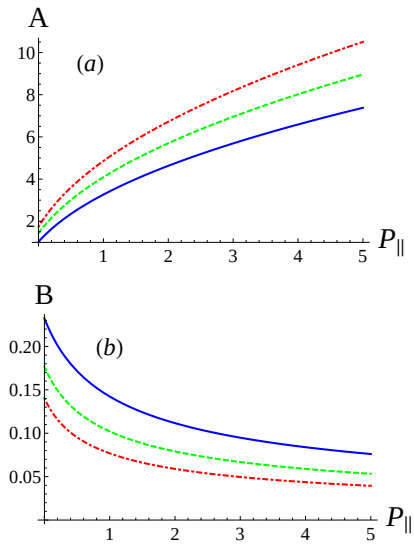

FIG. 7: Coefficients A and B versus $P_{\|}$, for different values of p. We have considered the values: $\kappa_e = \kappa_p = \kappa = 3$ and $\sigma_e = 1$. (a) A versus $P_{\|}$ for $p = 0$ (blue solid line), $p = 0.1$ (green dashed line) and $p = 0.2$ (red dot-dashed line); (b) B versus $P_{\|}$, for $p = 0$ (blue solid line), $p = 0.1$ (green dashed line) and $p = 0.2$ (red dot-dashed line).

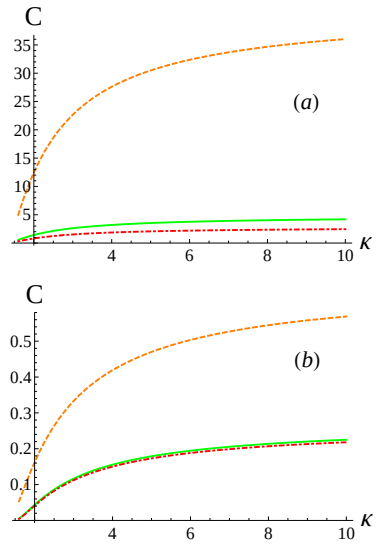

FIG. 6: Coefficient C versus κ for $P_{\|} = 0.3, P_{\perp} = 0.1, \sigma_e = 1$ and $p = 0.2$.
(a) C versus κ, based on Eq. (40), for values of $\Omega < 1$. The dashed (orange), solid (green) and dot-dashed (red) curves correspond to values of $\Omega = 0.1, 0.3$ and 0.4 respectively.
(b) C versus κ, based on Eq. (40), for values of $\Omega \geq 1$. The dashed (orange), solid (green) and dot-dashed (red) curves correspond to values of $\Omega = 1, 5$ and 7 respectively.

netic field through the frequency ratio Ω. In figure 6a we have shown how the coefficient C is influenced by the magnetic field in the presence of superthermal electrons and positrons, in the case of a weak magnetic field ($\Omega < 1$), while the analogous plots for a strong magnetic field ($\Omega \geq 1$) are provided in Figure 6b.

Anisotropy effect. The coefficients of the ZK equation are explicitly dependent on the parallel and perpendicular components of the ion pressure, $P_{\|}$ and $P_{\perp}$. In the following, we shall study the behavior of coefficients A and B against $P_{\|}$, and of C against $P_{\|}$ and $P_{\perp}$.

In Figure 7, we have depicted the dependence of A and B versus the ion parallel pressure $P_{\|}$, focusing on the effect of (varying) the positron concentration. Both coefficients A and B are strongly dependent on $P_{\|}$; it is seen that a higher positron content in the plasma makes A larger, but B smaller: positrons thus favor nonlinearity, against dispersion.

In Figure 8, we have plotted the coefficients A and B against $P_{\|}$, this time focusing on the superthermality effect. Stronger superthermality (lower κ values) reduces A but increases B.

The dispersive coefficient C depends on both $P_{\|}$ and $P_{\perp}$. In Figure 9, we have shown the effect of ion pressure anisotropy on coefficient C both in superthermal plasma as well as in Maxwellian plasma. The dependence of C on $P_{\perp}$ turns out to be stronger than on $P_{\|}$, as evident in Figure (9). On the other hand, C is significantly reduced as result of superthermality.

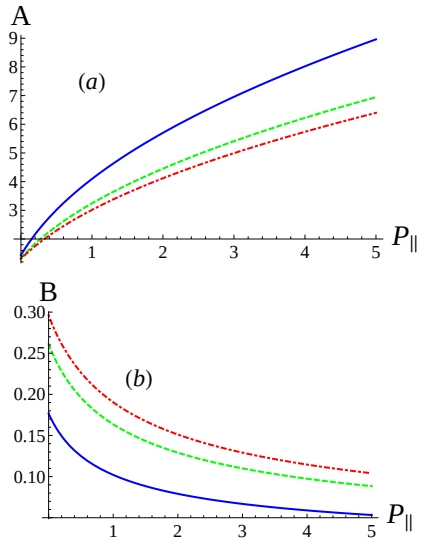

FIG. 8: Coefficients A and B versus $P_\parallel$, for different values of the superthermality index κ, taking $p = 0.1$ and $\sigma_e = 1$. (a) A versus $P_\parallel$ for $\kappa_e = \kappa_p = \kappa = 3$ (blue solid line), $\kappa_e = \kappa_p = \kappa = 5$ (green dashed line), $\kappa_e = \kappa_p = \kappa = 7$ (red dot-dashed line); (b) B versus $P_\parallel$ for $\kappa_e = \kappa_p = \kappa = 3$ (blue solid line), $\kappa_e = \kappa_p = \kappa = 5$ (green dashed line), $\kappa_e = \kappa_p = \kappa = 7$ (red dot-dashed line).

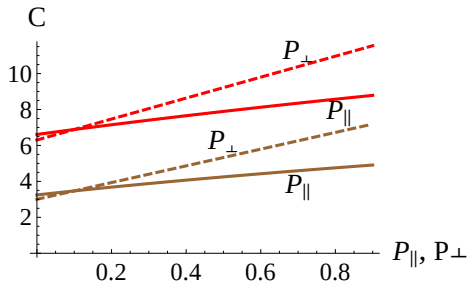

FIG. 9: Effect of $P_\parallel$ and $P_\perp$ on the coefficient C, for $p = 0$, $\Omega = 0.3$ and $\sigma_e = 1$. The bottom two (brown) curves are plotted with $\kappa_e = \kappa_p = \kappa = 3$, while the upper two (red) curves are plotted for a Maxwellian distribution function. In both top and bottom curve pairs, the values of $P_\parallel = 0.1$ (dashed lines) and $P_\perp = 0.1$ (solid lines) were considered.

VII. PULSE STABILITY ANALYSIS

In this section, we investigate the stability of the soliton pulse solution (44), following the method proposed by Allen and Rowlands (AR) in Ref. 74.

We have had to performed two distinct preliminary tasks, before proceeding with the AR method, properly speaking. First, using an appropriate scaling, we have reduced our ZK equation (39) to its "canonical" form; cf. Eq. (1.1) of Ref. 74. Details are given in the Appendix. It is obvious that this amounts to significant algebraic simplification, yet somewhat against physical transparency, in that important parameters (like Ω, for instance) are thus "hidden" in the variables, rather than the coefficients. Importantly, the space asymmetry which is induced by pressure anisotropy and by the magnetic field (direction) is also "obscured" by a variable transformation, in this way. We have therefore had to reverse back to the original variables, to ensure the consistency of our solitary wave solution (44) with Eq. (1.2) of Ref. 74, which is the solution of their (canonical) ZK equation; again, details are given in the Appendix.

Applying an appropriate transformation (see Appendix A), our ZK equation reduces to

$$\frac{\partial\hat{\Phi}}{\partial T'} + \hat{\Phi}\frac{\partial\hat{\Phi}}{\partial X'} + \frac{\partial}{\partial X'}\left(\frac{\partial^2\hat{\Phi}}{\partial^2 X'} + \frac{\partial^2\hat{\Phi}}{\partial^2 Y'}\right) = 0, \qquad (46)$$

which is exactly the same as Eq. (1.1) of Ref. 74, upon a trivial change in notation (formally setting $\hat{\Phi} = n$ therein).

Since a transformation exactly reduces our ZK equation to the form discussed in Ref. 74, we shall content ourselves to highlighting the main points of the stability investigation [74], without reproducing the derivations. The reader is referred to the original Ref. 74 for a detailed account of the algebra.

Following Allen and Rowlands, we have applied the following solution to Eq. (46)

$$\hat{\Phi} = \Phi_0 + \epsilon\Phi(x)\, e^{iky} e^{\gamma t}, \qquad (47)$$

where Φ_0 is the exact solution of Eq. (46), k is the wave vector (transverse direction), and γ is the measure of the growth rate of the instability (which occurs for $R_e\gamma \neq 0$.) The function $\Phi_{(x)}$ is determined by adopting a multiscale perturbation method, relying on an expansion in k (details can be found in Ref. 74).

In the limit of small k ($\ll 1$), the growth rate for instability is proportional to the real part of γ (i.e., $R_e\gamma$), can be written as:

$$\Gamma = k\gamma_1 + k^2\gamma_2 + ..., \qquad (48)$$

where γ_1 gives the instability up to first order, γ_2 gives the instability in second order, and so on. A lengthy calculation leads to

$$\gamma_1 = \frac{8}{3}\left[\left(\frac{8}{5}\cos^2\theta - 1\right)^{1/2} + i\sin\theta\right], \qquad (49)$$

where θ is the angle between the transverse component of the perturbation and the direction of the magnetic field. For instability to occur in first order, one must impose $\frac{8}{5}\cos^2\theta - 1 < 0$, thus $\theta > 37.8°$. The growth rate is then given by $\Gamma \simeq k\gamma_1 + \mathrm{O}(k^2)$.

If the configuration is stable up to first order ($\sim k$), i.e. assuming a small-angle perturbation ($\theta < 37.8°$), one may still have instability in the second order ($\sim k^2$);

the growth rate then reads: $\Gamma \simeq k^2\gamma_2 + \mathrm{O}(k^3)$ [74], with γ_2 given as:

$$\gamma_2 = -\frac{4}{9}\left(\frac{8}{5}\cos^2\theta - 1\right)\sec\theta + \frac{4(5+4\cos^2\theta)i\tan\theta}{45(\frac{8}{5}\cos^2\theta-1)^{1/2}}. \tag{50}$$

One can summarize the instability analysis of AR [74] for small k, in the following manner:

i) If $\theta < \theta_{cr} \simeq 37.8^\circ$, then the growth rate of the instability Γ is given by

$$\Gamma = \Gamma_1 = k\,R_e(\gamma_1) + \mathcal{O}(k^2) \simeq k\,\frac{8}{3}\left(\frac{8}{5}\cos^2\theta - 1\right)^{1/2}. \tag{51}$$

ii) If $\theta > \theta_{cr} \simeq 37.8^\circ$, then the growth rate is expressed as,

$$\Gamma = \Gamma_2 = k^2 R_e(\gamma_2) + \mathcal{O}(k^3) \simeq k^2\frac{4}{9}(1 - \frac{8}{5}\cos^2\theta)\sec\theta. \tag{52}$$

In order to obtain a working expression for the instability growth rate in terms of our physical model, we have to determine a transformation leading from eq. (46) back to our original ZK equation (39), namely relying on the scales $\Phi_0 = \frac{B}{L_\parallel^2 A}$, $T_0 = \frac{L_\parallel^3}{B}$, $L_\parallel$ and $L_\perp = L_\parallel\left(\frac{C}{B}\right)^{1/2}$, for Φ, time, x and y respectively. Using the above scaling, we have set (based on our model)

$$k \to kL_\perp, \qquad \gamma_1 \to \gamma_1 T_0 \qquad \gamma_2 \to \gamma_2 T_0, \tag{53}$$

to cast equations (51) and (52) into the form

$$\Gamma = \Gamma_1 \simeq k\frac{(BC)^{1/2}}{L_\parallel^2}\frac{8}{3}\left(\frac{8}{5}\cos^2\theta - 1\right)^{1/2} \tag{54}$$

and

$$\Gamma = \Gamma_2 \simeq k^2\frac{C}{L_\parallel}\frac{4}{9}\left(1 - \frac{8}{5}\cos^2\theta\right)\sec\theta \tag{55}$$

respectively. In the above algebraic steps, B and C are as defined earlier, and $L_\parallel \in \Re$ is left arbitrary in the algebra (in fact, is typically corresponds to the Debye length, qualitatively speaking).

We have numerically studied the dependence of the growth rate of the instability on our plasma parameters, namely κ, p, $P_\parallel$ and $P_\perp$. In Figure 10, we have depicted the growth rate Γ_1 versus θ, based on Eq. (54), focusing on the effect of the electron and positron superthermality (index) κ, on the positron content (through the density ratio p) and on the ion pressure anisotropy (through $P_\parallel$ and $P_\perp$). It is clear from Figure 10 that the growth Γ_1 goes to zero as $\theta \to \theta_{cr} = 37.8^\circ$. However, for smaller values of θ ($0 \le \theta < 37.8^\circ$), increasing superthermality (i.e., reducing the value of κ) shrinks down the growth rate: deviation from the Maxwellian distribution seems to suppress the instability therefore; see Fig. 10b. An increase in the positron population (higher p) bears the same effect, namely it suppresses the instability; see Fig. 10c. One can see in Figure 10c that the ion parallel pressure $P_\parallel$ bears a negligible effect on the growth rate (Γ_1). On the other hand, increasing $P_\perp$ enhances the growth rate.

In an analogous manner, in Figure 11 we have plotted the second order instability growth rate Γ_2 versus θ based on Eq. (55). One can see that the growth rate (Γ_2) increases sharply beyond $\theta > 37.8^\circ$, yet the quantitative effect of our plasma parameters κ, p, $P_\parallel$ and $P_\perp$ appears to be small saturates at large θ.

VIII. CONCLUSIONS

In this article, we have investigated the propagation characteristics of ion acoustic excitations in magnetized plasma characterized by inertialess suprathermal electrons and positrons, and warm anisotropic ions. Both linear (waves) and nonlinear (pulses) structures were considered. The anisotropy in terms of the ion pressure tensor asymmetry is modeled through CGL theory [2]. In the linear regime, we have obtained two dispersion curves, corresponding to magnetized ion acoustic and ion cyclotron modes in e-p-i plasma. The linear analysis can be summarized as:

– Increasing the superthermality parameter (κ) of electron and positron causes both electrostatic modes (i.e., ion acoustic and ion cyclotron) to propagate at higher phase velocity.

– By increasing the positron population through $p = \frac{n_{p0}}{n_{i0}}$, the frequency of both modes decreases i.e., increasing positrons in the system make waves slower.

– Increasing the magnetic field strength through $\Omega = \frac{\Omega_i}{\omega_{pi}}$, the phase velocities also increases.

- For fixed perpendicular pressure component $P_\perp$, increasing the parallel pressure element $P_\parallel$ enhances the phase velocity in both modes. On the other hand, fixing $P_\parallel$ and increasing $P_\perp$ increases the frequency of the upper mode, while the acoustic mode is slowed down.

In the nonlinear regime, we have considered localized perturbations in a two-dimensional geometry. We have employed a reductive perturbation method to derive a Zakharov-Kuznetsov (ZK-)type equation, which admits a pulse-shaped solitary wave solution, whose form is reminiscent of a KdV soliton. It is found that only compressive solitary structures are supported. The results of a parametric analysis of the solitary wave solution thus obtained can be summarized as:

- The solitary wave (pulse) speed depends on the superthermality parameter (κ), and on the parallel pressure $P_\parallel$, but is independent of the perpendicular pressure $P_\perp$.

- The coefficient of nonlinearity (A) and the coefficient of parallel dispersion B (relative to the magnetic field) depend parametrically on the parallel pressure $P_\parallel$, on the positron content p and on superthermality ($\kappa_{e,p}$), and is thus independent of the perpendicular pressure. Hence the perpendicular pressure component $P_\perp$ has no effect

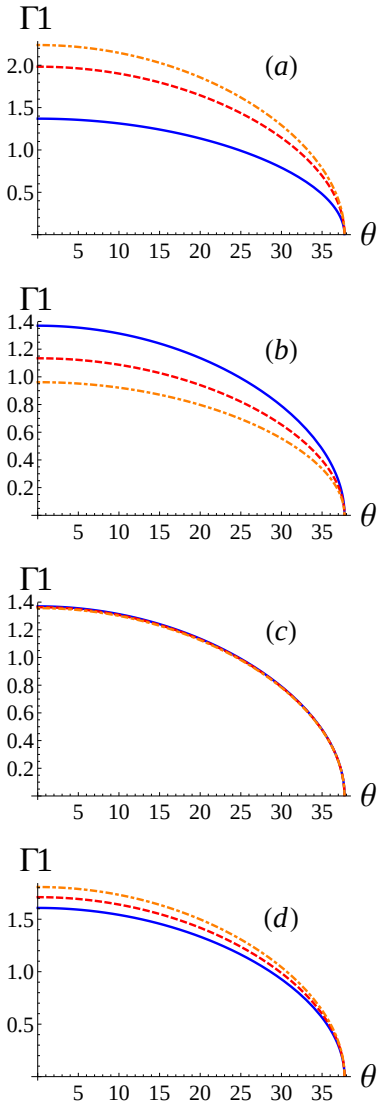

FIG. 10: The first-order instability growth rate (Γ_1) has been computed, here shown versus θ, based on Eq. (54) for $k_y = 0.05$, $L_\parallel = 0.2$, $\sigma = 1$ and $\Omega = 0.3$. The values here considered are:
(a) $P_\parallel = 0.3, P_\perp = 0.1, p = 0.2$ and $\kappa_e = \kappa_p = \kappa = 3$ (blue solid curve); $\kappa_e = \kappa_p = \kappa = 5$ (red dashed curve); $\kappa_e = \kappa_p = \kappa = 7$ (orange dot-dashed curve).
(b) $P_\parallel = 0.3, P_\perp = 0.1, \kappa_e = \kappa_p = \kappa = 3$ and $p = 0.2$ (blue solid curve); $p = 0.3$ (red dashed curve); $p = 0.4$ (orange dot-dashed).
(c) $p = 0.2, \kappa_e = \kappa_p = \kappa = 3, P_\perp = 0.1$ and $P_\parallel = 0.3$, (blue solid curve); $P_\parallel = 0.5$ (red dashed curve); $P_\parallel = 0.9$ (orange dot-dashed).
(d) $p = 0.2, \kappa_e = \kappa_p = \kappa = 3, P_\parallel = 0.1$ and $P_\perp = 0.3$, (blue solid curve); $P_\perp = 0.4$ (red dashed curve); $P_\perp = 0.5$ (orange dot-dashed).

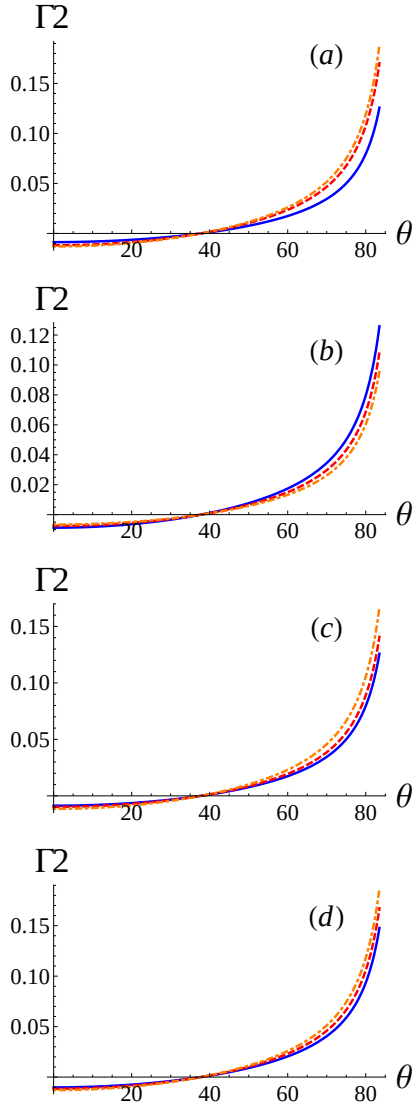

FIG. 11: The second-order instability growth rate (Γ_2) has been computed, here shown versus θ, based on Eq. (55) for $k_y = 0.05, L_\parallel = 0.2, \sigma = 1, \Omega = 0.3$. The parameter values adopted are:
(a) $P_\parallel = 0.3, P_\perp = 0.1, p = 0.2$ and $\kappa_e = \kappa_p = \kappa = 3$ (blue solid curve); $\kappa_e = \kappa_p = \kappa = 5$ (red dashed curve); $\kappa_e = \kappa_p = \kappa = 7$ (orange dot-dashed curve).
(b) $P_\parallel = 0.3, P_\perp = 0.1, \kappa_e = \kappa_p = \kappa = 3$ and $p = 0.2$ (blue solid curve); $p = 0.3$ (red dashed curve); $p = 0.4$ (orange dot-dashed).
(c) $p = 0.2, \kappa_e = \kappa_p = \kappa = 3, P_\perp = 0.1$ and $P_\parallel = 0.3$, (blue solid curve); $P_\parallel = 0.5$ (red dashed curve); $P_\parallel = 0.9$ (orange dot-dashed).
(d) Γ_2 versus θ for $p = 0.2, \kappa_e = \kappa_p = \kappa = 3, P_\parallel = 0.1$ and $P_\perp = 0.3$, (blue solid curve); $P_\perp = 0.4$ (red dashed curve); $P_\perp = 0.5$ (orange dot-dashed).

on the amplitude of solitary waves. On the other hand, the coefficient of perpendicular dispersion (C) does depend on $P_\perp$ and on the magnetic field strength (through Ω). We have noticed that coefficient C is more sensitive to $P_\perp$ rather than the parallel pressure $P_\parallel$, hence the width of the solitary waves (W) is more sensitive to the perpendicular pressure.

- The amplitude of the solitary waves remains essentially unaffected by varying the magnetic field strength, however the width of the soliton decreases with increasing the magnetic field strength and the width approaches to a constant profile for very large magnetic field ($\Omega > 1$).

We have also carried out a stability analysis of the solitary wave solution, following the method by Allen and Rowlands [74]. The following facts arise from the analysis:

- The first order instability growth rate (Γ_1) decreases with θ (i.e., the angle between the transverse component of the perturbation and the direction of the magnetic field) in the range ($0 \leq \theta < 37.8^\circ$). An increase in the perpendicular ion pressure $P_\perp$ leads to an increase in the growth rate Γ_1. On the other hand, if one increases the positron population (through p) the growth rate (Γ_1) becomes smaller, while the parallel ion pressure $P_\parallel$ has practically no effects on Γ_1. Finally, by increasing the deviation from the Maxwellian (higher superthermality, i.e. for smaller κ), one finds that the instability is suppressed.

- We have also investigated the parametric effect of relevant parameters on the second order instability growth rate Γ_2: the growth rate increases sharply beyond $\theta > 37.8^\circ$, while the effect of the plasma parameters saturates at large θ.

Our work is motivated by a series of magnetosheath observations made by instruments onboard two spacecraft, namely AMPET/CCF and AMPET/IRM, as described in Denton *et al* [5], and partly by the work of Seough *et al* [26]. Pressure anisotropy also has an essential role in the turbulent intracluster medium (ICM) as discussed by Nakwacki *et al* [61]. They showed that in a low density collisionless medium, such as ICM the thermal pressure become anisotropic with respect to the magnetic field orientation and lead to the evolution of the turbulent gas. The favorable condition for ion pressure anisotropy in such plasma environments is that the ion gyrofrequency is much larger than the ion-ion collision frequency. Our results may provide a good qualitative description of the observations of solitary waves in various space and astrophysical environments possessing strong magnetic fields, particularly to the magnetosphere and near earth's magnetosheath [4, 5, 61], where non-thermal electrons with ion pressure anisotropy can exist.

Acknowledgments

M.A. warmly acknowledges the Higher Education Commision (HEC), Islamabad, Pakistan for financial support under the Indigenous PhD 5000 and IRSIP Fellowship Programs. I.K. acknowledges financial support from European Union (EU) via an FP7/IRSES grant ("QUANTUM PLASMAS - Complex ideal and non-ideal quantum plasmas", PIRSES-GA-2013-612506), and from CNPq (Conselho Nacional de Desenvolvimento Científico e Tecnológico), Brazil. Instituto de Física, Universidade Federal do Rio Grande do Sul (UFRGS), Porto Alegre Brazil is also warmly acknowledged for its hospitality, during the latter stages of this work.

APPENDIX A: ANALYTICAL TRANSFORMATION OF EQ. (39) TO EQ. (46)

Our ZK equation (39), as derived for two dimensional electrostatic perturbations in the plasma, is given by:

$$\frac{\partial \Phi_1}{\partial \tau} + A\Phi_1 \frac{\partial \Phi_1}{\partial X} + \frac{\partial}{\partial X}\left(B\frac{\partial^2 \Phi_1}{\partial^2 X} + C\frac{\partial^2 \Phi_1}{\partial^2 Y}\right) = 0. \quad \text{(A1)}$$

Let us introduce a scaling normalization (normalization):

$$\Phi_1 \to \Phi_0 \Phi', \qquad \tau \to T_0 T^{'}, \qquad X \to L_\parallel X^{'}, \qquad Y \to L_\perp Y^{'}, \quad \text{(A2)}$$

where the primed variables are dimensionless, and all other quantities are scaling quantities to be determined. By using the above transformation, Eq. (A1) is transformed into a similar equation, in structure (in terms of the primed quantities), yet with

$$A \to A' = \frac{A\Phi_0 T_0}{L_\parallel}, B \to B' = \frac{BT_0}{L_\parallel^3}, C \to C' = \frac{CT_0}{L_\parallel L_\perp^2}.$$

The requirement $A' = B' = C' = 1$ (in view of casting the ZK equation in its canonical form) imposes:

$$\Phi_0 = \frac{B}{L_\parallel^2 A}, \qquad T_0 = \frac{L_\parallel^3}{B}, \qquad L_\perp = L_\parallel \left(\frac{C}{B}\right)^{1/2},$$

where $L_\parallel \in \Re$ is left arbitrary, formally, at this stage (physically, it is thought of as of the order of the ion Debye length $\lambda_{Di} = \left(k_B T_e / 4\pi n_{i0} e^2\right)^{1/2}$ in our case, though this need not be taken into account in the forthcoming algebra). The above manipulations allow us to cast Eq. (A1) above into the form of (46).

Upon formally setting $\Phi' \to n$, one obtains:

$$\frac{\partial n}{\partial T'} + n\frac{\partial n}{\partial X'} + \nabla^2\left(\frac{\partial n}{\partial X'}\right) = 0,$$

which is precisely Eq. (1.1) of Ref. [74].

APPENDIX B: ANALYTICAL TRANSFORMATION OF EQ. (44) TO EQ. (1.2) OF REF. [69]

Our starting point is relation (44):

$$\Phi_1 = \left(\frac{3u_0}{l_x A}\right) \mathrm{sech}^2(\chi\,(l_x X + l_y Y - u_0 \tau)).$$

Considering

$$\Phi_1 \rightarrow \Phi_0\hat{\Phi}, \quad \tau \rightarrow T_0T^{'}, \quad X \rightarrow L_{\parallel}X^{'}, \quad Y \rightarrow L_{\perp}Y^{'},$$

and adopting the scaling in (A2) above, the above expression is transformed into (1.2) in Ref. [74]. Substituting with $u_0 \rightarrow \frac{4\eta^2 Bl_x}{L_{\parallel}^2}$ and restricting the propagation to only along the magnetic field, viz., $l_x = 1$ and $l_y = 0$ one obtains

$$\Phi_0 = 12\eta^2 \mathrm{sech}^2\left[\eta X - 4\eta^3 t\right],$$

which is precisely the sought after expression.

[1] W. Baumjohann and R. A. Treumann *Basic Space Plasma Physics* (Imperial College Press, London, 1997).
[2] G.F. Chew, M.L. Goldberger, F.E. Low, Proc. R. Soc. London **A236,** 112 (1956)
[3] G. K. Parks *Physics of Space Plasmas* (Perseus USA, 1991).
[4] R.E. Denton, B.J. Anderson, S.P. Gary, S.A. Fuselier, J. Geophys. Res. **99**, (A6)11 (1994)
[5] C.R. Choi, C-Mo. Ryu, D.Y. Lee, N.C. Lee, Y.H. Kim, Phys. Lett. A **364**, 297 (2007)
[6] V.M. Vasyliunas, J. Geophys. Res. **73**, 2839-2884 (1968)
[7] A. Hasegawa, K. Mima, M. Duong-van, Phys. Rev. Lett. **54**, 2608-2610 (1985)
[8] V. Pierrard, J. Lemaire, J. Lorentzian, J. Geophys. Res. **101**, 7923-7934 (1996)
[9] V. Pierrard, H. Lamy,J. Lemaire, J. Geophys. Res. **109**, A02118 (2004)
[10] M.A. Hellberg, R.L. Mace, R.J. Armstrong, G. Karlstad, Phys. Plasmas **64**, 433-443 (2000)
[11] M.V. Goldman, D.L. Newman, A. Mangeney, Phys. Rev. Lett. **99**, 145002 (2007)
[12] A. Olsson, P. Janhune, Ann. Geophys. **16**, 298-302 (1998)
[13] S.P. Christon, D.J. Williams, D.G. Mitchell, L.A. Frank, Y. Huang, J. Geophys. Res. **94,** 13409-13424 (1989)
[14] M.P. Leubner, Z. Voros, J. Astrophys. **618**, 547-555 (2005)
[15] B.A. Shrauner, W.C. Feldman, J. Plasma Phys. **17**, 123-131 (1977)
[16] S. Sultana, G. Sarri, I. Kourakis, Phys. Plasmas **19**, 012310 (2012)
[17] S. Devanandhan, S.V. Singh, G.S. Lakhina, R. Bharuthram, Nonlin. Processes Geophys. **18**, 627–634 (2011)
[18] C.-R. Choi, K.-W. Min, T.-N. Rhee, Phys. Plasmas **18**, 092901 (2011)
[19] A. Shah, R. Saeed, Plasma Phys. Control. Fusion **53**, 095006 (2011)
[20] N.S. Saini, I. Kourakis, M. A. Hellberg, Phys. Plasmas **16**, 062903 (2009)
[21] S. Sultana, I. Kourakis, Plasma Phys. Control. Fusion **53,** 045003 (2011)
[22] R. Sabry, W.M. Moslem, P.K. Shukla, Astrophysics. Space Sci. **333**, 203-208 (2011)
[23] G. Williams, I. Kourakis, Plasma Phys. & Cont. Fusion **55**, 055005 (2013)
[24] S.V. Singh, S. Devanandhan, G.S. Lakhina, R. Bharuthram, Phys. Plasmas **20**, 012306 (2013)
[25] X. Meng, G. Toth, I. Sokolov, T. Gombosi, J. Comp. Phys. **231**, 3610 (2012)
[26] J. Seough, P.H. Yoon, K. Kim, D. Lee, Phys. Rev. Lett **110**, 071103 (2013)
[27] S.I. Popel, S.V. Vladimirov, P.K. Shukla, Phys. Plasmas **2**, 716 (1995)
[28] S. Mahmood, A. Mushtaq, H. Saleem, New J. Phys. **5**, 28 (2003)
[29] H.P. Pakzad, Astrophys. Space Sci. **334**, 337 (2011)
[30] B. Sahu, Astrophys. Space Sci. **338**, 251 (2012)
[31] H. Alinejad, S. Sobhanian and J. Mahmoodi, Phys. Plasmas **13**, 012304 (2006)
[32] E.I. El-Awady, S.A. El-Tantawy, W.M. Moslem, P. K. Shukla, Phys. Lett. A **374**, 3216 (2010)
[33] F.C. Michel, Rev. Mod. Phys. **54**, 1 (1982)
[34] H.R. Miller, P. J. Witta, *Active Galactive Nuclei, p. 202.* (Springer, Berlin 1987)
[35] B. Kozlovsky, R.J. Murphy, G.H. Share, Astrophys. J. **604**, 892 (2004)
[36] E.P. Liang, S.C. Wilks, M. Tabak, Phys. Rev. Lett. **81**, 4890 (1998)
[37] C.M. Surko, T.J. Murphy, Phys. Fluids **2**, 1372 (1990)
[38] R.G. Greaves, M.D. Tinkle, C. M. Surko, Phys. Plasmas **1**, 1439 (1994)
[39] M. Tinkle, R.G. Greaves, C.M. Surko, R.L. Spencer and G.W. Mason, Phys. Rev. Lett., **72**, 352 (1994)
[40] R.G. Greaves, C.M. Surko, Phys. Rev. Lett., **75**, 3846 (1995)
[41] G. Gahn, G.D. Tsakiris, G. Pretzler, K.J. Witte, C. Delfin, C.G. Wahlstrom, D. Habs, Appl. Phys. Lett., **77**, 2662 (2000)
[42] Y.B. Zel'dovich, I.D. Novikov, *Relativistic Astrophysics*, University of Chicago Press, Chicago, IL (1981)
[43] S.L. Shapiro, S.A. Teakolsky, *Black Holes, White Dwarfs and Neutron Stars: The Physics of Compact Objects*, Wiley-Interscience, New York (1983)
[44] G. Sarri, W. Schumaker, A. Di Piazza, M. Vargas, B. Dromey, M.E. Dieckmann, V. Chvykov, A. Maksimchuk, V. Yanovsky, Z.H. He, B.X. Hou, J.A. Nees, A.G.R. Thomas, C.H. Keitel, M. Zepf, K. Krushelnick, Phys. Rev. Lett., **110**, 255002 (2013)
[45] H. Chen, M. Nakai, Y. Sentoku, Y. Arikawa, H. Azechi, S. Fujioka, C. Keane, S. Kojima, W. Goldstein, B.R. Maddox, N. Miyanaga, T. Morita, T. Nagai, H. Nishimura, T. Ozaki, J. Park, Y. Sakawa, H. Takabe, G. Williams, Z. Zhang, New J. Phys., **15**, 065010 (2013)
[46] E.P. Liang, S.C. Wilks, M. Tabak, Phys. Rev. Lett., **81**, 4887 (1998)
[47] H. Chen, S.C. Wilks, J.D. Bonlie, E.P. Liang, J. Myatt, D.F. Price, D.D. Meyerhofer and P. Beiersdorfer, Phys. Rev. Lett., **102**, 105001 (2009)
[48] B. Shen, J. Meyer-ter-Vehn, J. Phys. Rev. E, **65**, 016405 (2001)
[49] S.C. Wilks, J.M. Dawson, W.B. Mori, Phys. Rev. Lett., **69**, 1383 (1992)
[50] J.W. Shearer, J. Garrison, J. Wong, J.E. Swain, Phys. Rev. A, **8**, 1582 (1973)

[51] N.L. Tsintsadze, R. Chaudhary, A. Rasheed, J. Plasma. Phys., **79**, 587 (2013)

[52] G. Sarri, 2013, private communication.

[53] O. Adriani, G.C. Barbarino, G. A. Bazilevskaya, et al, Nature **458**, 607 (2009)

[54] A.M. Galper, S.V. Koldashov, V.V. Mikhailov, S.A. Voronov, Radiat. Meas. **26**, 375 (1996)

[55] S.A. Voronov, A.M. Galper, V.G. Kirilov-Ugryumov, S.V. Koldashov, A.V. Popov, JETP Lett. 43, 307 (1986)

[56] E. Fiandrini, J. Geophys. Res. **108**, 1402 (2003)

[57] J.L. Hortwitz, D.L. Gallagher, W.K. Peterson, *Geospace Mass and Energy Flow*, p. 343. AGU, Washington (1998)

[58] F. Verheest, T. Cattaert, M. Hellberg, Space Sci. Rev. **121**, 299 (2005)

[59] M. Tribeche, K. Aoutou, S. Younsi, M. Amour, Phys. Plasmas **16**, 072103 (2009)

[60] E.F. El-Shamy, W.F. El-Taibany, E.K. El-Shewy, El-Shorbagy, Astrophys. Space Sci. **338**, 279 (2012)

[61] M.S. Nakwacki, E.M. Gouveia Dal Pino, G. Kowal, R. Santos-Lima, Journal of Physics, Conference Series **370**, 012043 (2012)

[62] M. Adnan, S. Mahmood, A. Qamar, Advances in Space Research **53,** 845 (2014)

[63] F.F. Chen, *Introduction to Plasma Physics and Controlled Fusion* (Plenum, New York, 1984)

[64] Yashvir et al, Plasma Phys. & Cont. Fussion **26**, 1303 (1984)

[65] H. Washimi, T. Tanuiti Phys. Rev. Lett. **17**, 996 (1966)

[66] E. Infeld, G. Rowlands *Nonlinear waves, solitons and chaos* (Cambridge University Press, 2000)

[67] W. Malfliet, J. Comput. Appl. Math. **164**, 529 (2004)

[68] I. Kourakis, W.M. Moslem, U.M. Abdelsalam, R. Sabry, P.K. Shukla, Plasma Phys. Control. Fusion **4**, 018 (2009)

[69] **J. Srinivas, S. I. Popel, and P. K. Shukla,J. Plasma Phys. 55, 209 (1996).**

[70] **G. Lu, Y. Liu, Y. Wang, L. Stenflo, S. I. Popel, and M. Y. Yu, J. Plasma Phys. 76, 267 (2010).**

[71] **F. Verheest and M. A. Hellberg, Electrostatic Solitons and Sagdeev Pseudopotentials in Space Plasmas: Review of Recent Advances, in: Handbook of Solitons (Eds: S.P. Lang and S.H. Bedore), pp. 353-392 (2009).**

[72] **F. Verheest, G. S. Lakhina and M. A. Hellberg Plasma Phys. 21, 062303 (2014).**

[73] **S. Sultana, I. Kourakis and M. A. Hellberg Plasma Phys. Cont. Fusion 54, 105016 (2012); DOI: 10.1088/0741-3335/54/10/105016.**

[74] M.A. Allen, G. Rowlands, J. Plasma Phy. **53**, 63 (1995)